ARTICLES
https://doi.org/10.1038/s41593-019-0523-z
nature neuroscience

Memory retrieval modulates spatial tuning of single neurons in the human entorhinal cortex

Salman E. Qasim[1], Jonathan Miller[1], Cory S. Inman[2], Robert E. Gross[2], Jon T. Willie[2], Bradley Lega[3], Jui-Jui Lin[3], Ashwini Sharan[4], Chengyuan Wu[4], Michael R. Sperling[5,6], Sameer A. Sheth[7], Guy M. McKhann[8], Elliot H. Smith[9], Catherine Schevon[10], Joel M. Stein[11] and Joshua Jacobs[1*]

The medial temporal lobe is critical for both spatial navigation and memory. Although single neurons in the medial temporal lobe activate to represent locations in the environment during navigation, how this spatial tuning relates to memory for events involving those locations remains unclear. We examined memory-related changes in spatial tuning by recording single-neuron activity from neurosurgical patients performing a virtual-reality object–location memory task. We identified 'memory-trace cells' with activity that was spatially tuned to the retrieved location of the specific object that participants were cued to remember. Memory-trace cells in the entorhinal cortex, in particular, encoded discriminable representations of different memories through a memory-specific rate code. These findings indicate that single neurons in the human entorhinal cortex change their spatial tuning to target relevant memories for retrieval.

A key feature of memory is our ability to selectively recall particular experiences even if they occurred in a setting shared with other events. For example, if a person is asked to recommend a tourist itinerary for a city they have visited frequently, they can selectively recall distinct memories of locations from different trips to provide an answer. Although lesion studies have demonstrated that many declarative memory processes depend on intact medial temporal lobe (MTL) structures, such as the hippocampus and entorhinal cortex[1,2], how neuronal activity in these regions enables the targeting of a particular memory for retrieval among related experiences is not clear.

We examined how the brain represents distinct memories through the lens of spatial cognition, relying on the fact that the brain uses similar circuits and mechanisms to support both spatial and memory processes[3,4]. The discovery of place cells in the hippocampus[5] and grid cells in the entorhinal cortex[6] demonstrates that neurons in these memory-critical regions[2] also exhibit spatial tuning. Previous work proposed that spatially tuned cells remap their firing patterns across different environments, so events that occur in different environments are associated with different spatial maps[7,8]. Recent work has extended the idea that different contexts are associated with different spatial maps by showing that the activity of spatially tuned cells may be modulated by changes to internal, top-down processes such as the behavioral state, attention, or goal of an animal[9–11]. In this way, different patterns of spatially modulated neuronal activity may index different behavioral and cognitive contexts, and these distinct neural representations may aid in the retrieval of distinct memories.

The entorhinal cortex is a viable candidate for linking memory retrieval to spatial representation[12], as it features a variety of spatially tuned cells[6,13], plays a role in memory maintenance and retrieval[14,15], and integrates diverse sensory and cognitive information about an experience in service of memory[16,17]. Recent work has begun to link memory processes with spatial firing patterns in the entorhinal cortex, such as the identification of object-trace cells in the rodent entorhinal cortex, in which spatial tuning was determined by the locations previously occupied by objects[18], the finding of reduced grid-cell representations in patients at risk for Alzheimer's disease[19], and the discovery that remembered reward locations influence grid-cell field locations[20].

Building on this work, we proposed that single neurons in the MTL, and particularly in the entorhinal cortex, would exhibit spatial tuning modulated by past experiences. Such separable neuronal representations may, in turn, enable top-down, targeted memory retrieval of those past experiences. To test this, we analyzed the activity of single neurons from the MTL of human epilepsy patients as they performed a cued spatial memory task in which they learned and subsequently recalled object locations while moving through a virtual environment. A key feature of this task was that participants were provided a cue in each trial denoting the specific object location to retrieve, while the environment remained unchanged. This enabled the assessment of how top-down, targeted memory retrieval might engage distinct spatial representations in the brain. We observed single neurons, largely in the entorhinal cortex, with spatial tuning that varied as a function of the particular cue provided for memory retrieval. Specifically, the activity of these cells tracked the subjective memory of the patient for the current cued object location; hence, we refer to them as 'memory-trace cells'. Furthermore, the firing of entorhinal cortex memory-trace cells showed a memory-specific rate code that distinguished which

[1]Department of Biomedical Engineering, Columbia University, New York, NY, USA. [2]Department of Neurological Surgery, Emory University, Atlanta, GA, USA. [3]Department of Neurological Surgery, University of Texas Southwestern, Dallas, TX, USA. [4]Department of Neurological Surgery, Thomas Jefferson University, Philadelphia, PA, USA. [5]Department of Neurology, Thomas Jefferson University, Philadelphia, PA, USA. [6]Jefferson Comprehensive Epilepsy Center, Jefferson University Hospitals, Philadelphia, PA, USA. [7]Department of Neurological Surgery, Baylor College of Medicine, Houston, TX, USA. [8]Department of Neurological Surgery, Columbia University, New York, NY, USA. [9]Department of Neurosurgery, University of Utah, Salt Lake City, UT, USA. [10]Department of Neurology, Columbia University, New York, NY, USA. [11]Department of Radiology, University of Pennsylvania, Philadelphia, PA, USA. *e-mail: joshua.jacobs@columbia.edu

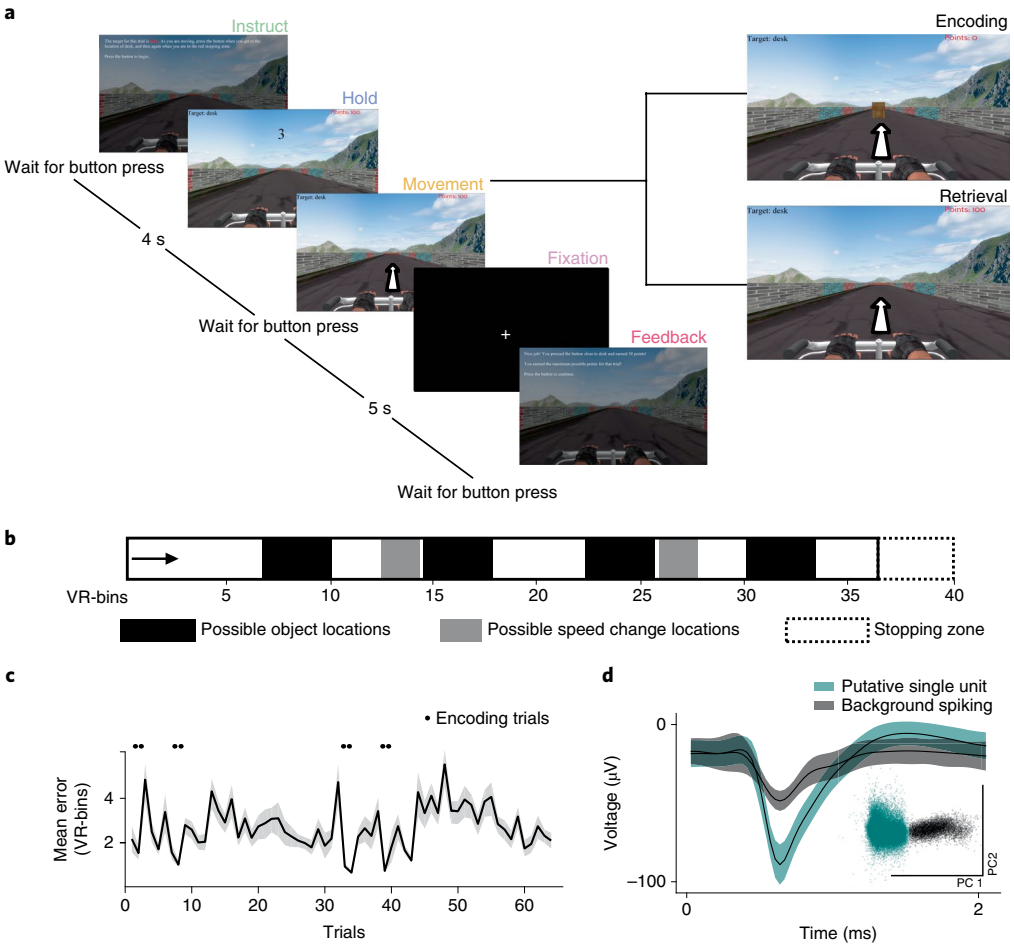

Fig. 1 | Task overview. a, Timeline of the object–location memory task. Inset indicates that movement periods either consist of encoding or retrieval epochs. **b**, An overhead map of the environment. Arrow represents the starting point of each trial. **c**, Mean response error in retrieval trials, averaged over all task sessions ($n = 31$ total sessions). Shading indicates s.e.m. **d**, Example putative single-unit waveform ($n = 6{,}887$ spikes) and example sub-threshold background spiking ($n = 78{,}872$ spikes). Solid lines indicate mean waveform; shading indicates s.e.m. Inset shows separation of waveform principal components (PCs), whereby one cluster represents the putative single-unit waveform and the other represents the background spiking.

object–location memory had been cued for retrieval. This memory-specific rate code was robust, emerging both when participants were near the location of the cued objects and when participants were provided with a retrieval cue but did not move through the environment. These findings illustrate how spatially tuned neurons in the entorhinal cortex support the ability to use top-down cues to selectively target relevant memories for retrieval.

Results

We recorded from 299 neurons in the entorhinal cortex, hippocampus, amygdala, and cingulate cortex of 19 neurosurgical patients who performed an object–location memory task (Fig. 1a and Supplementary Figs. 1,2). In this task, participants were instructed to learn the locations of different objects along a virtual linear track and then to recall the locations after the objects were removed. The task consisted of separate encoding and retrieval trials, which followed the same general structure except that objects were visible on the track during encoding trials and absent during retrieval trials. Each trial began with an instruction period, in which participants viewed the name of the cued object for that trial. This was followed by the hold period, during which participants remained stationary at the entrance to the track for 4 s. Next was the movement period, in which the participant was moved automatically down the track at randomly varying speeds. During encoding trials, the object was present on the track, enabling the subject to press a button as they reached the visible location of the object (Fig. 1b). During retrieval trials, the object was absent and the participant pressed a button at the location in which they remembered the cued object being present (Supplementary Video 1). Participants generally showed high accuracy during retrieval trials, pressing the button within 2.8 virtual units (VR-bins) of the correct location, or 7% of the track length, on average (Fig. 1c).

We examined how the activity of individual neurons (see Fig. 1d for example) represented the spatial location of participants in the task by computing the firing rate of each neuron as a function of the position of the participant along the track during retrieval trials. To assess the modulation of neuronal activity, we used a two-way repeated-measure analysis of variance (ANOVA) to identify neurons for which activity during retrieval trials varied as a function of the location of the participant (1–40 spatial bins), the retrieval cue (1–4 possible cues), and their interaction, determining significance using a permutation procedure. As we describe below, this analysis revealed two groups of neurons with distinct firing patterns (Fig. 2). We found neurons with firing rates that varied as a function of only participant location, similar to conventional place cells[5,21]. We also found neurons, which we refer to as memory-trace cells, with spatial tuning that shifted along the track depending on the retrieval cue viewed by the participant at the beginning of each trial.

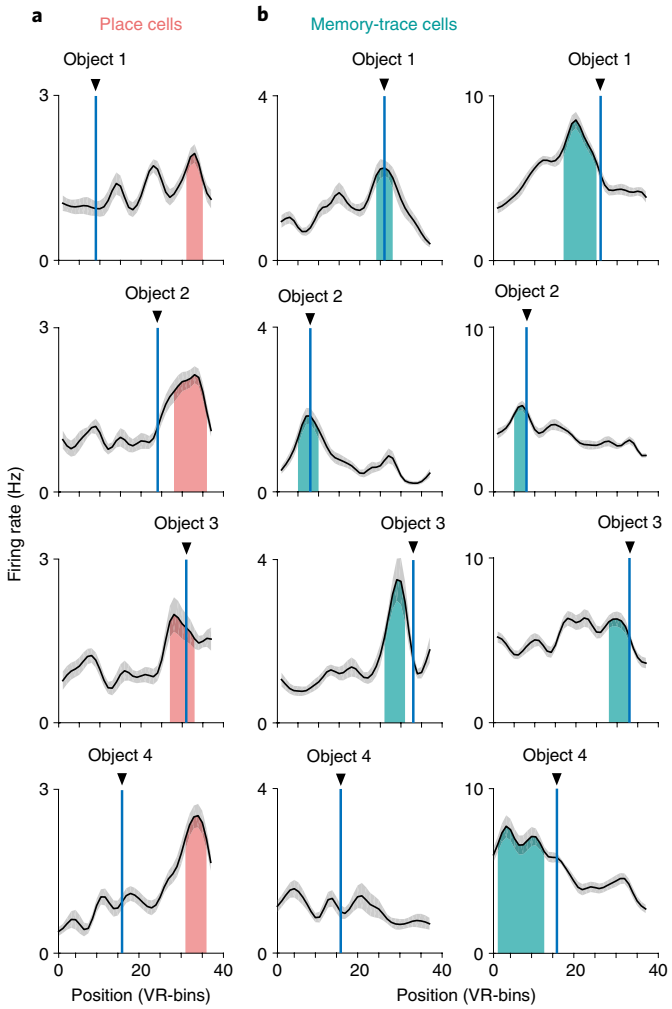

Fig. 2 | Examples of place and memory-trace cells. a, The mean firing rate (black lines, $n = 12$ trials per block) of an example hippocampal place cell. Individual plots show the activity for trial blocks with different cue objects. Vertical blue lines indicate object locations. Gray shading indicates s.e.m. Colored region indicates place fields determined by finding contiguous bins with elevated firing rates (see Methods). **b**, The activity of two entorhinal cortex memory-trace cells. Note that, in contrast to the place cells in **a**, the firing fields of these cells (shaded regions) shift depending on the retrieval cue.

Place cells activate in fixed locations, independent of memory retrieval demands. We identified place cells as those that showed a significant main effect of location on firing rate and had at least one place field (Fig. 3, see Methods). A significant number of cells (50 of 299, $P = 8.78 \times 10^{-14}$, binomial test versus 5% chance) fulfilled our criteria as place cells. Most place fields were smaller than 10% of the track length and none covered more than 40% of the track (Fig. 3c).

We found significant numbers of place cells in the entorhinal cortex, hippocampus, and cingulate (Fig. 3d, all P values $< 10^{-4}$, binomial test versus 5% chance). To examine the possibility that these findings were the result of neuronal responses to time[22] or speed[23], we used an analysis of covariance (ANCOVA) to test whether the location-related modulation of these cells persisted after including speed and time as covariates[24]. Almost all (90%) of place cells still exhibited significant spatial coding after accounting for potential effects of time or speed, indicating that their activity primarily reflected the spatial location of the participant.

Spatial tuning of memory-trace cells shifts according to the retrieval cue. In contrast to place cells, Fig. 2b depicts the activity of two example entorhinal cortex memory-trace cells, with spatial tuning that shifted depending on the particular object–location cue viewed by the participant at the beginning of each trial. We identified memory-trace cells systematically as those cells that showed significantly increased firing in contiguous spatial bins for at least one cue, which we refer to as 'trace fields' (see Methods), and that had a spatial firing pattern that shifted significantly across different cues (determined via a location × cue interaction in the ANOVA). Overall, a significant number of cells (43 of 299, $P = 6.37 \times 10^{-10}$, binomial test versus 5% chance) fulfilled the criteria for memory-trace cells (Supplementary Figs. 3,4). These cells were found primarily in the entorhinal and cingulate cortices (Fig. 4a, P values $< 10^{-5}$, binomial tests versus 5% chance). We observed at least one memory-trace cell in 15 of 19 participants (Supplementary Table 1); 12 of 19 participants exhibited both place and memory-trace cells.

Individual memory-trace cells exhibited a unique trace field for between one and four cues (Fig. 4b and Supplementary Fig. 4), distinguishing them from cue-association cells in primates[25], which responded to only a single association. Specifically, the firing of many memory-trace cells shifted to represent multiple locations over the course of a session, often appearing to fire near the location of the object cued for each trial.

To determine whether memory-trace cell activity reflected underlying memory retrieval processes, we next examined whether the spatial tuning of these neurons was more strongly anchored to the response location (where the participant believed the object to be) rather than the true location of the object[26]. If this were the case then realigning memory-trace cell firing relative to the response location would yield a stronger pattern of spatially modulated firing than the pattern observed when realigning firing rate relative to the location of the object. We tested this by quantifying the spatial information[27], a measure of the specificity of the spatial tuning, in both the response- and object-aligned configurations for each of the four cues. Spatial information was significantly greater in the response-aligned configuration than in the object-aligned configuration (Fig. 4c, sign-rank test, $z = 3.4$, $P = 0.0007$), suggesting that memory-trace cell firing represents the location of the participant relative to the location targeted for memory retrieval.

Memory-trace cell activity tracks subjective memory for cued object locations during retrieval. Having determined that memory-trace cells were more strongly spatially tuned in response-aligned configurations, we next assessed in more detail where these cells fired in relation to the location of participant responses. As shown in Fig. 5a, trace fields clustered in the spatial bins immediately preceding the response, appearing on average 2.5 VR-bins before the response location ($t(125) = -2.09$, $P = 0.038$). This suggested that trace-field activity signaled the relevance of a location for upcoming memory retrieval[28]. Furthermore, trace fields appeared significantly closer to the response locations of the participants than the true object location in a given trial ($t(1495) = 1.79$, $P = 0.037$). To confirm this preference for locations preceding the response, we computed the grand average of memory-trace cell firing rates in the spatial locations surrounding the response (Fig. 5b). This confirmed that memory-trace cells generally increased their firing as participants approached the response location, and then decreased following the response (paired t-test pre- versus post-firing rate, $t(1986) = 3.99$, $P = 6.73 \times 10^{-25}$; Supplementary Fig. 5). The broad peak and gradual decline in average firing rate across memory-trace cells depicted in Fig. 5b reflects the heterogeneity of trace-field offsets relative to the response location (Fig. 5a), as opposed to all trace fields appearing at the same offset.

To further test whether memory-trace cell activity tracks subjective memory we analyzed the memory-trace cell firing rate in

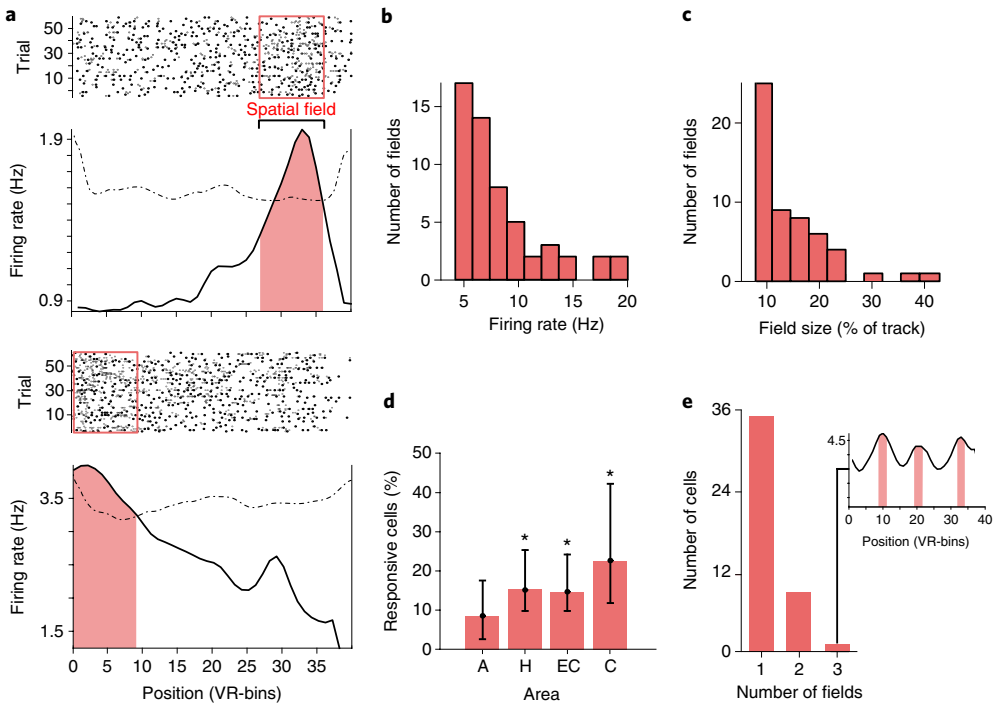

Fig. 3 | Place cell activity. a, Raster plot and mean firing rate for two example place cells recorded from the hippocampus. Box and shading indicate place fields. Dotted line represents the threshold for identifying place fields, assessed non-parametrically (see Methods). **b**, Distribution of mean firing rates among place fields. **c**, Distribution of field sizes across all place cells, expressed as a percentage of the track. **d**, Proportion of place cells recorded in each brain area. A, amygdala ($n=62$ cells); H, hippocampus ($n=97$ cells); EC, entorhinal cortex ($n=113$ cells); C, cingulate ($n=27$ cells). Asterisks (*) indicate significant proportions (P values all $<10^{-4}$, two-sided binomial test versus 5% chance). Error bars indicate the 95% confidence interval from a binomial test. **e**, Number of responsive cells with more than one spatial field. Inset shows an example cell from the cingulate that showed three spatial fields.

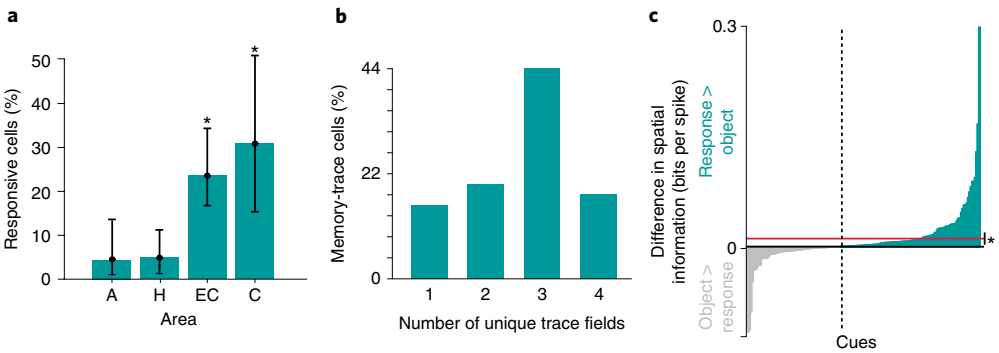

Fig. 4 | Trace-fields shift according to memory for cued object locations. a, Distribution of memory-trace cells across brain areas. A, amygdala ($n=62$ cells); H, hippocampus ($n=97$ cells); EC, entorhinal cortex ($n=113$ cells); C, cingulate ($n=27$ cells). Asterisks (*) indicate significant proportions ($P<10^{-5}$, two-sided binomial test versus 5% chance). Error bars indicate the 95% confidence interval from a binomial test. **b**, Distribution of the counts of unique trace fields exhibited by memory-trace cells. **c**, Difference in spatial information for the firing rate of each memory-trace cell for each cue ($n=168$ cues), when aligned relative to response location versus object location. Asterisk (*) indicates significance ($z=3.4$, $P=0.0007$, signed-rank test).

retrieval trials in which participants made large errors (16.8% of trials). These trials enabled us to dissociate participant response location and the actual object location. By comparing the response- and object-aligned firing rates during these trials, we found that the firing of these cells peaked significantly closer to the response location than the actual object location (Fig. 5c, $t(333)=2.13$, $P=0.033$). These results further support the idea that memory-trace cell spatial tuning is anchored to the retrieval of the location of a cued object from memory.

Because cells in the MTL have shown evidence of coding for time[22], we considered the possibility that memory-trace cells were firing at specific timepoints, rather than spatial offsets, relative to the response (Supplementary Fig. 6). We therefore performed an analysis comparing the extent to which individual memory-trace cell activity was predicted as a function of distance or time relative to the response. This analysis revealed that the firing rates of memory-trace cells were more strongly predicted by the spatial rather than temporal offset ($t(42)=2.35$, $P=0.024$), supporting the idea that memory-trace cell activity represents the distance to upcoming recalled locations.

We next sought to better understand the type of distance-to-memory information represented by memory-trace cells. We examined

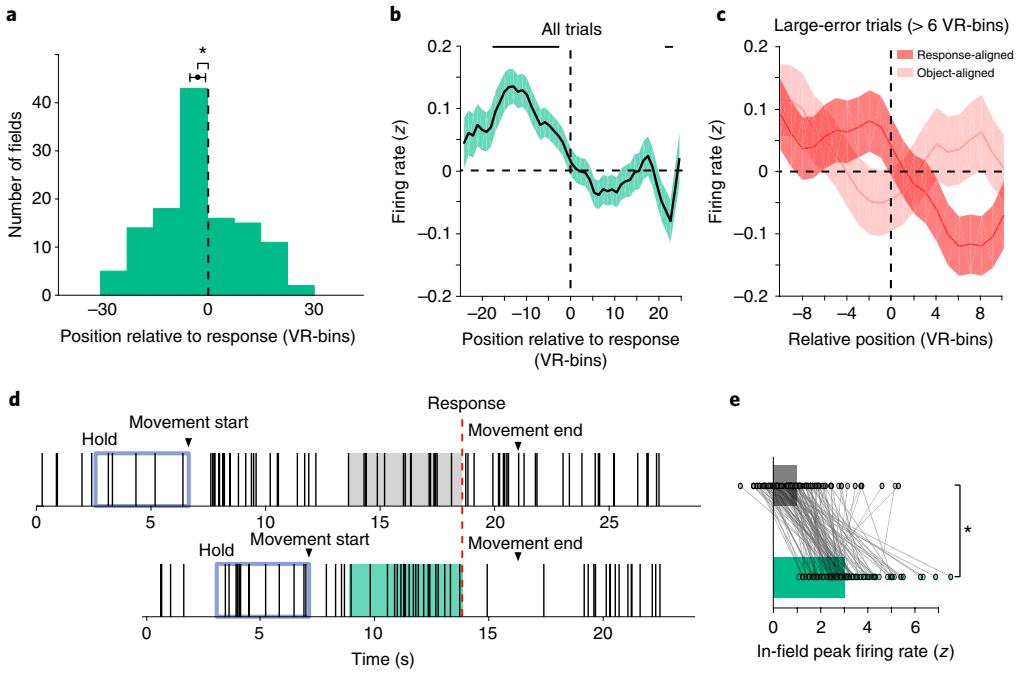

Fig. 5 | Memory-trace cells track subjective memory during retrieval. a, Distribution of trace-field locations ($n = 126$ trace fields across 43 memory-trace cells) relative to response location (indicated by black dashed line). Asterisk (*) indicates that the mean field location significantly precedes response location ($t(125) = 2.09$, $P = 0.038$, two-sided t-test). **b**, Mean firing rate during retrieval trials (z-scored) of all memory-trace cells (black line, $n = 1{,}990$ trials) aligned to response location. Shading indicates s.e.m. Horizontal lines indicate spatial bins that are significantly different from baseline (P values < 0.05, two-sided t-test, false discovery rate (FDR)-corrected). **c**, Mean firing rate (z-scored) of all memory-trace cells during large-error trials (solid lines, $n = 334$ trials), aligned to response location (dark red) or object location (light red). Shading indicates s.e.m. **d**, Example spike trains from a single entorhinal cortex memory-trace cell during an example encoding (top) and retrieval (bottom) trial for the same cued location. Vertical lines denote spike times. Responses were aligned and shaded (5 s pre-response) to qualitatively illustrate the difference in spiking between trial types. **e**, Population data showing greater memory-trace cell peak firing rate in-field (z-scored) during retrieval than encoding trials, as visualized by the example in panel **d** ($t(125) = 12.92$, $P = 8.95 \times 10^{-25}$, two-sided t-test). Circles denote data from individual trace fields ($n = 126$).

whether memory-trace cell firing fields appeared at fixed offsets from the response location, as might be expected from a general distance code for relevant locations[11], or whether they appeared at cue-specific distances, as might be expected in a form of goal-oriented remapping[10]. We conducted an analysis of trace-field offset consistency across cues (Supplementary Fig. 7), and found that a significant number of memory-trace cells had trace fields at reliably fixed offsets across cues (5 of 37 cells with more than one trace field, $P = 0.036$, binomial test versus 5% chance), whereas a different but equally prevalent subset of cells (5 of 37 cells) showed significantly variable offsets across cues.

To further determine whether the activity of memory-trace cells specifically relates to memory retrieval, we examined their firing patterns in encoding trials, in which the cued object was visible. Comparing neural activity between encoding and retrieval trials (which were perceptually identical apart from the visible object) enabled the identification of specific features of memory-trace cell responses that related to memory retrieval, while controlling for other factors that differed across trials, such as object identity[16], goal locations[11,29], and motor planning[30]. Overall, we found that, when a participant was located in the firing field of a memory-trace cell, there was increased activity in retrieval trials compared to encoding trials ($t(125) = 12.9$, $P = 8.9 \times 10^{-24}$; Fig. 5d,e). To assess whether memory-trace cells simply fired in the same locations during encoding trials but with lower firing rates than in retrieval trials, we computed the spatial correlation between the memory-trace cell firing patterns during retrieval and encoding (see Methods and Supplementary Fig. 8). Memory-trace cell spatial firing patterns were largely uncorrelated between encoding and retrieval trials ($\chi^2(1) = 149.35$, $P < 2.2 \times 10^{-16}$), meaning that the spatial tuning observed during retrieval was not present at lower firing rates during encoding. By contrast, place cells exhibited significantly more stable spatial tuning between encoding and retrieval trials than memory-trace cells (Supplementary Fig. 9, Mann-Whitney U-test, $z = 5.25$, $P = 1.48 \times 10^{-7}$). These results indicate that, during encoding, memory-trace cells either shift spatial tuning or are simply inactive, providing evidence in favor of the idea that the observed memory-trace cell spatial tuning uniquely supports memory retrieval. Furthermore, we found no effect of low versus high measures of attention on memory-trace cell activity (see Methods, $F_{(1, 639)} = 0.16$ and 0.48; P values > 0.05, permutation test), indicating that attention probably did not explain the differences between encoding and retrieval. This is consistent with findings indicating that attentional mechanisms do not fundamentally differ between encoding and retrieval[31].

In summary, memory-trace cell spatial tuning was predominantly modulated by the response location of the participant specifically during cued memory retrieval. This pattern was robust even when participant responses were inaccurate, suggesting that memory-trace cells tracked the participants' internal representation of the location of the cued object.

Activity of memory-trace cells in the entorhinal cortex separably and robustly represents different memories. Although the above analyses showed that the activity of memory-trace cells tracked retrieved locations in the environment, whether these cells support memory representations more generally beyond moving through the relevant environment remained unclear. Understanding this

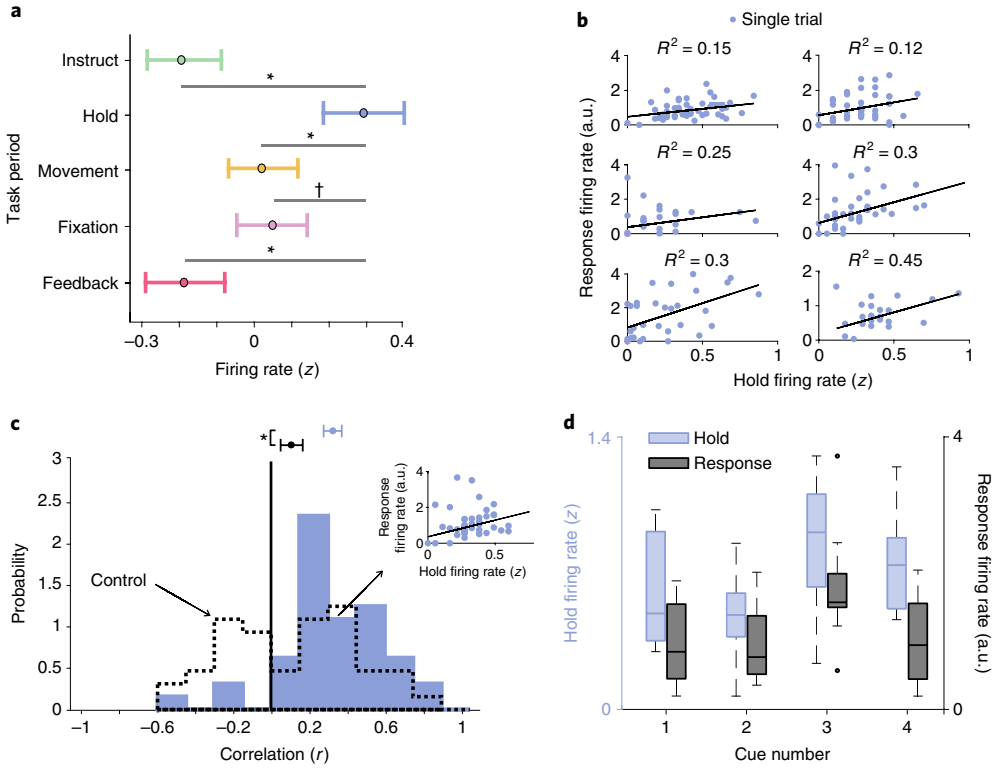

Fig. 6 | Memory-trace cell activity is correlated between the hold period and response period. a, Mean normalized (*z*-scored) firing rate (circles) across all memory-trace cells by task period ($n = 1{,}990$ trials). Error bars indicate s.e.m. *$P < 0.05$ (FDR-corrected two-sided *t*-tests); †$P < 0.1$. **b**, Relation of firing rates between hold and response periods for six example memory-trace cells. Black line denotes the robust linear regression fit. a.u. denotes arbitrary units, indicating that the response period activity is defined by a ratio (of pre- versus post-response firing rate). Each plot depicts 48 retrieval trials, except the middle-left and bottom-right plots, which depict sessions with 24 trials. **c**, Distribution of Pearson correlation coefficients for memory-trace cell firing rates between hold and response periods ($n = 43$ cells). Inset shows correlation for one example cell. Circles indicate mean, and error bars indicate s.e.m. Dotted line denotes control distribution (see Methods). Asterisk (*) indicates significant difference ($t(42) = 2.99$, $P = 0.0046$, two-sided *t*-test). **d**, Normalized firing rate during hold and response periods for each object cue for an example entorhinal cortex memory-trace cell. Center line indicates median, box limits indicate interquartile range, whiskers indicate 1.5× interquartile range ($n = 12$ trials). Circles indicate outliers.

could help to explain how humans are able to remotely recall events from outside the environment in which they occurred. We investigated this question by analyzing memory-trace cell activity during the hold period of our task, which follows the initial viewing of the retrieval cue during the instruction period. We proposed that, during the hold period, participants would exhibit similar neural representations of the current memory retrieval cue to those exhibited when moving through the target location in the environment. We therefore investigated whether the same patterns of neuronal activity associated with retrieval of particular memories during movement also emerged during the hold period. Overall, memory-trace cell firing rates were significantly elevated during the hold period of retrieval trials (Fig. 6a, $F_{(4,\ 10075)} = 2.88$, $P = 0.021$, post hoc *t*-tests, *P* values < 0.05, FDR-corrected). This effect was not seen during encoding trials, or in non-trace cells (Supplementary Fig. 10). This indicates that memory-trace cells were generally engaged during the hold period, although participants were still, rather than moving through the environment.

We proposed that memory-trace cell activity during the hold period would correlate with memory-trace cell activity when participants remembered the location during movement. This correlation might indicate that memory-trace cell representations for retrieved locations generalize beyond memory retrieval during movement, supporting the potential use of such representations for retrieval across multiple contexts. To facilitate comparison of memory-trace cell firing rates across the hold period and the response location, we first characterized the changes in firing rate in the spatial bins surrounding the response location (Fig. 5b), which we called the response period. We measured the magnitude of the response-modulated changes in memory-trace cell activity by normalizing the pre-response firing rate of each cell by its post-response firing rate. This accounted for the background activity of each neuron and helped to ensure that correlations computed between the hold and response periods of a trial would not be confounded by overall trial-wide increases in firing rate. For each cell, we then computed the correlation across trials between the firing rates during the hold and response periods (Fig. 6b). We compared this measure to the correlation in firing rate between the hold period and a matched control period, which did not include the response (see Methods). We found that memory-trace cell firing positively correlated between the hold and response periods, and not between the hold and control periods (Fig. 6c and Supplementary Fig. 11a), indicating that a consistent pattern of neuronal activity for individual cues was present during the hold and response periods (see Fig. 6d and Supplementary Fig. 11b for examples). Firing rates during these periods did not correlate with task performance (Supplementary Fig. 12).

We next used a multivariate cross-decoding analysis[32] to more fully characterize how the neural representations of specific memories that emerged during the response period were recapitulated across various task periods (see Methods, Supplementary Fig. 13). Here we trained separate decoders to predict the currently cued object location memory from the normalized firing rates of the population of memory-trace cells for each task period. We then tested the decoding performance of each model on activity from the

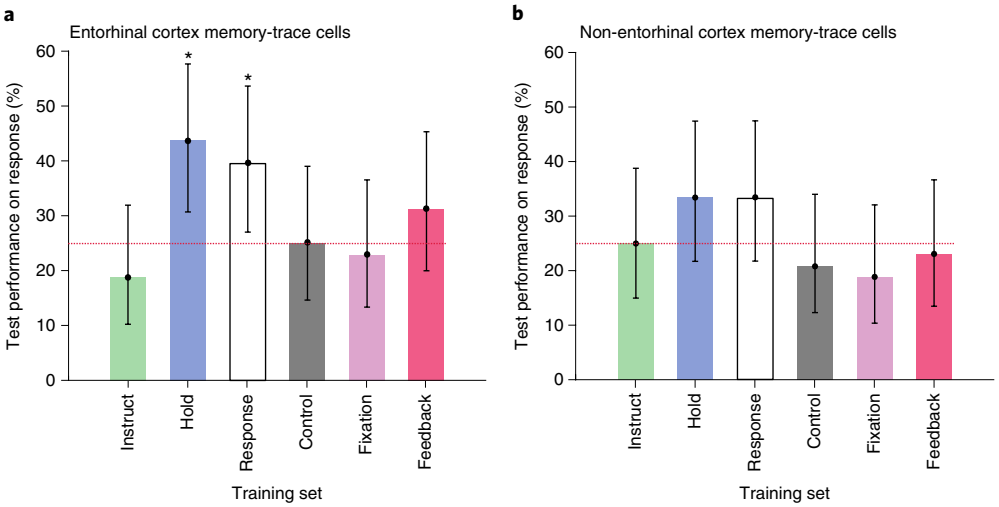

Fig. 7 | Entorhinal cortex memory-trace cell activity predicts cued memory across hold and response periods. a, Results of memory-decoding analysis for entorhinal cortex memory-trace cells ($n = 27$). Individual bars distinguish models that were trained on different task periods, with all models tested on activity during the response period. Bar height denotes testing performance, and error bars indicate the 95% confidence interval from a binomial test. Dotted line indicates chance-level performance (25%). Asterisks (*) indicate above-chance decoding accuracy (P values < 0.05, two-sided binomial tests). **b**, Test performance for decoders based on non-entorhinal cortex memory-trace cell firing ($n = 16$), with training on each of the task periods and testing on the response period.

response period. In this analysis, if we were to observe that a model trained on one period demonstrated elevated decoding performance when tested on memory-trace cell firing during the response period, then it would indicate that the neural representations of specific memories were similar between these two periods.

The results of this analysis indicated that the firing rates of entorhinal cortex memory-trace cells represented individual memory cues similarly between the hold and response periods. For entorhinal cortex memory-trace cells, when comparing test performance in the response period for various training models, only the model trained on the hold period showed significantly increased accuracy (Fig. 7a, $P = 0.0043$, binomial test versus 25% chance). This pattern was not present for memory-trace cells outside the entorhinal cortex (Fig. 7b). Additionally, we observed significant decoding from entorhinal memory-trace cells when models were both trained and tested on the response period using tenfold cross-validation (Fig. 7a; $P = 0.029$, binomial test), which confirms the reliability of these patterns. To characterize the patterns of memory-related neural activity across the task more fully, we also performed a complete cross-decoding analysis, in which we compared the performance of training and testing models across all pairs of task periods (Supplementary Fig. 14c). In particular, we did not find significant cross-decoding for data from the control period. This indicates that entorhinal cortex memory-trace cells do not represent the currently cued memory when the participant is far from the target location. Furthermore, to test whether these patterns were robust, we also individually applied this cross-decoding analysis to the first and second halves of each session, but we found that decoding performance did not differ between the halves (all P values > 0.05, χ^2 test). Overall, these results demonstrate that entorhinal cortex memory-trace cells exhibit a distinctive firing-rate code for individual memory cues that is consistent both during the hold period and when the participant moves through the associated target location.

Discussion

A crucial aspect of human memory is the ability to actively target and differentiate between past experiences. Here we show that the activity of entorhinal cortex memory-trace cells selectively represents and differentiates between memories from a single environment. Critically, memory-trace cells represent information about locations that participants had been cued to remember, illustrating how top-down memory demands influence the representation of space in the brain. Our observations suggest that memory-trace cell activity represents object locations that a person is trying to remember. The activity of entorhinal cortex memory-trace cells, specifically, was predictive of the cued memory both during the stationary hold period and when participants moved through retrieved locations, suggesting that these cells support a generalizable and robust memory-specific representation. Our findings therefore indicate that, in addition to the fixed metric for space provided by grid cells[6,13], the human entorhinal cortex also contains neurons that support a flexible spatial code modulated by top-down memory demands. Below, we discuss how memory-trace cells relate to previous single-cell findings in the hippocampus and entorhinal cortex relevant to space and memory, and how they help to explain the broader role of the entorhinal cortex in the memory network of the brain.

Place cells in the hippocampus are thought to represent a map of the current environment, and evidence shows that these representations remap in response to changes to the environment[33,34]. This led to the idea that different environmental contexts induce orthogonal spatial representations in these cells, which are used to index different maps for past experiences[7,8]. The phenomenon of goal-oriented remapping, in which place fields change location or accumulate near goal locations without changes to local cues or spatial context, or both, demonstrates that top-down influence and goal-driven behavior can modulate spatial firing[9,10]. A significant proportion of memory-trace cells exhibited firing fields at different offsets from the response location depending on the cue being retrieved, demonstrating a potential link to goal-oriented remapping and suggesting that the link between remapping and memory-trace cell activity should be further investigated. Furthermore, distal CA1 place cells—which receive direct entorhinal cortex input—show partial remapping based on the presence and location of objects in the environment[35], raising the possibility that entorhinal cortex memory-trace cells also influence or interact with hippocampal remapping. Future work should investigate the relationship between our findings and remapping, and how these phenomena interact in service of memory.

That memory-trace cell activity tracked the current cued memory indicates that top-down memory retrieval states influenced the firing of these cells. Related work has found cells that represent goal-related spatial information in the hippocampal formation of rodents and bats[11,29,36]. The key distinction between memory-trace cells and these other cell types is that memory-trace cells do not significantly activate when objects, the putative goal, are visible in the environment. As such, memory-trace cell activity is probably more specifically related to memory retrieval processes, rather than goal coding in general. Interestingly, some specific properties of memory-trace cells recapitulate elements of these goal-coding cells. Specifically, goal cells in the rodent subiculum also fire in locations preceding rewards[11], and goal representations in bats[29] are also maintained even when the goal is occluded. Additionally, some memory-trace cells exhibited firing fields at fixed offsets from the response location independent of the cue, providing a potential link to hippocampal goal-vector coding. Future work that more extensively measures memory-trace cell activity relative to visible goals may characterize their similarity to goal cells.

Our finding that memory-trace cells in the entorhinal cortex, in particular, exhibited consistently decodable representations of individual object–location memories extends previous work documenting the role of the entorhinal cortex in the representation of object features and context in rodents and non-human primates[16,37]. Specifically, our findings bear significant resemblance to 'object-trace cells' discovered in the rodent entorhinal cortex[18] and cingulate[38]. Rodent object-trace cells activated in locations in which animals had previously encountered objects and could represent a non-specific, putative trace of all the objects encountered by the rodent in the environment. However, human memory-trace cells had two crucial additional features that were not observed in rodents. The activity of memory-trace cells specifically tracked the location recalled by participants, indicating that the top-down memory target modulated spatial tuning, rather than showing increased activity for all previous object–locations as in rodent object-trace cells. Additionally, memory-trace cells exhibited a memory-specific rate code even when participants were not moving through the environment.

This prevalence of memory-trace cells in the entorhinal cortex may advance our understanding of the functional role of the entorhinal region in memory. Recent work using neuromodulation has demonstrated a causal role for the entorhinal cortex in human spatial and episodic memory[39,40]. Additionally, the entorhinal cortex is thought to be an early staging ground for the onset of Alzheimer's disease[41,42], with evidence suggesting that the spread of Alzheimer's pathology begins in the entorhinal cortex[43] and that entorhinal tau is directly linked to memory decline in old age[44]. Given these lines of research, one possibility is that the memory-trace cells we identified are affected by stimulation or lesion of the entorhinal cortex, resulting in these subsequent effects on memory. Indeed, recent work has shown that mice expressing tau pathology in the entorhinal cortex showed concomitant spatial memory deficits and major loss of cells in entorhinal cortex layers II and III, providing evidence of a potential link between loss of memory-related cells in the entorhinal cortex (such as memory-trace cells) and memory deficits[45].

Additionally, recent work in humans has shown that the activity of grid cells is degraded in people at risk for Alzheimer's disease[19], and correlates with spatial memory performance[46,47]. It is possible that grid cells and memory-trace cells both contribute to entorhinal cortex memory circuits, and the relationship between them may be important to understand how spatial and memory processes interact in the entorhinal cortex. Indeed, two recent studies in rodents discovered that grid-cell maps shift to represent remembered reward locations, suggesting the influence of task-relevant variables on the structure of entorhinal spatial maps[20,48]. Our findings build on this work by demonstrating a specific way in which top-down processes may interact with flexible spatial representations to index events for memory retrieval in the entorhinal cortex.

We found a small but significant proportion of memory-trace cells in the cingulate cortex in addition to the entorhinal cortex. Our previous work identified grid-like single-neuron activity in the cingulate cortex of humans, in addition to the entorhinal cortex[13], which complement related findings from functional magnetic resonance imaging (fMRI) showing grid representations outside of the entorhinal cortex[46]. The colocalization of memory-trace cells and grid cells suggests that these cells represent a common memory network involving both the entorhinal cortex and the cingulate cortex. Going forward, further exploration of the relationship between memory-trace cells and grid cells may provide insights into the neural mechanisms underlying spatial and mnemonic function across regions.

In conclusion, we demonstrate the existence of memory-trace cells that flexibly change their spatial tuning to distinguish individual memories during retrieval. Entorhinal cortex memory-trace cells exhibited consistent activity across the hold and response periods of our task, enabling the decoding of cued memories and indicating that entorhinal cortex representations persist beyond purely spatial or navigational settings. This supports the idea that the entorhinal cortex is important for general relational and contextual memory representations[16,17]. Looking forward, although our results focus on how memory modulates spatial tuning to distinguish subjective memory representations, other emerging lines of work now show that the entorhinal cortex maps non-spatial features of experience[49,50]. Our findings may therefore enable new lines of investigation in various species of how entorhinal neuronal representations of space and other domains are modulated by top-down demands in service of memory and other high-level cognitive processes.

Online content

Any methods, additional references, Nature Research reporting summaries, source data, extended data, supplementary information, acknowledgements, peer review information, details of author contributions and competing interests, and statements of code and data availability are available at https://doi.org/10.1038/s41593-019-0523-z.

Received: 17 October 2018; Accepted: 23 September 2019;
Published online: 11 November 2019

References

1. Scoville, W. B. & Milner, B. Loss of recent memory after bilateral hippocampal lesions. *J. Neurol. Neurosurg. Psychiatry* **20**, 11–21 (1957).
2. Squire, L. R., Knowlton, B. & Musen, G. The structure and organization of memory. *Annu. Rev. Psychol.* **44**, 453–495 (1993).
3. O'Keefe, J. & Nadel, L. *The Hippocampus as a Cognitive Map*. (Oxford University Press, 1978).
4. Buzsaki, G. & Moser, E. Memory, navigation and theta rhythm in the hippocampal–entorhinal system. *Nat. Neurosci.* **16**, 130–138 (2013).
5. O'Keefe, J. & Dostrovsky, J. The hippocampus as a spatial map: preliminary evidence from unit activity in the freely-moving rat. *Brain Res.* **34**, 171–175 (1971).
6. Hafting, T., Fyhn, M., Molden, S., Moser, M.-B. & Moser, E. I. Microstructure of a spatial map in the entorhinal cortex. *Nature* **436**, 801–806 (2005).
7. Leutgeb, S., Leutgeb, J. K., Treves, A., Moser, M.-B. & Moser, E. I. Distinct ensemble codes in hippocampal areas CA3 and CA1. *Science* **305**, 1295–1298 (2004).
8. Colgin, L., Moser, E. & Moser, M. Understanding memory through hippocampal remapping. *Trends Neurosci.* **31**, 469–477 (2008).
9. Markus, E. J. et al. Interactions between location and task affect the spatial and directional firing of hippocampal neurons. *J. Neurosci.* **15**, 7079 (1995).
10. Dupret, D., O'Neill, J., Pleydell-Bouverie, B. & Csicsvari, J. The reorganization and reactivation of hippocampal maps predict spatial memory performance. *Nat. Neurosci.* **13**, 995–1002 (2010).
11. Gauthier, J. L. & Tank, D. W. A dedicated population for reward coding in the hippocampus. *Neuron* **99**, 179–193.e7 (2018).

12. Sugar, J. & Moser, M.-B. Episodic memory: neuronal codes for what, where, and when. *Hippocampus* https://doi.org/10.1002/hipo.23132 (2019).
13. Jacobs, J. et al. Direct recordings of grid-like neuronal activity in human spatial navigation. *Nat. Neurosci.* **16**, 1188–1190 (2013).
14. Brun, V. et al. Place cells and place recognition maintained by direct entorhinal-hippocampal circuitry. *Science* **296**, 2243 (2002).
15. Chao, O. Y., Huston, J. P., Li, J.-S., Wang, A.-L. & de Souza Silva, M. A. The medial prefrontal cortex-lateral entorhinal cortex circuit is essential for episodic-like memory and associative object-recognition. *Hippocampus* **26**, 633–645 (2016).
16. Knierim, J. J., Neunuebel, J. P. & Deshmukh, S. S. Functional correlates of the lateral and medial entorhinal cortex: objects, path integration and local-global reference frames. *Philos. Trans. R. Soc. Lond. B Biol. Sci.* **369**, 20130369 (2014).
17. Behrens, T. E. J. et al. What is a cognitive map? Organizing knowledge for flexible behavior. *Neuron* **100**, 490–509 (2018).
18. Tsao, A., Moser, M.-B. & Moser, E. I. Traces of experience in the lateral entorhinal cortex. *Curr. Biol.* **23**, 399–405 (2013).
19. Kunz, L. et al. Reduced grid-cell–like representations in adults at genetic risk for Alzheimer's disease. *Science* **350**, 430–433 (2015).
20. Butler, W. N., Hardcastle, K. & Giocomo, L. M. Remembered reward locations restructure entorhinal spatial maps. *Science* **363**, 1447–1452 (2019).
21. Ekstrom, A. D. et al. Cellular networks underlying human spatial navigation. *Nature* **425**, 184–187 (2003).
22. Kraus, B. J. et al. During running in place, grid cells integrate elapsed time and distance run. *Neuron* **88**, 578–589 (2015).
23. Kropff, E., Carmichael, J. E., Moser, M.-B. & Moser, E. I. Speed cells in the medial entorhinal cortex. *Nature* **523**, 419–424 (2015).
24. Robitsek, R., White, J. & Eichenbaum, H. Place cell activation predicts subsequent memory. *Behavioural Brain Res.* **254**, 65–72 (2013).
25. Sakai, K. & Miyashita, Y. Neural organization for the long-term memory of paired associates. *Nature* **354**, 152–155 (1991).
26. O'Keefe, J. & Speakman, A. Single unit activity in the rat hippocampus during a spatial memory task. *Exp. Brain Res* **68**, 1–27 (1987).
27. Skaggs, W. E, McNaughton, B. L, Gothard, K. M. & Markus, E. J. (eds Hanson, S. J., Cowan, J. D. & Giles, C. L.,). An information-theoretic approach to deciphering the hippocampal code. *Adv. Neural Inf. Process. Syst.* **5**, 1030–1037 (1993).
28. Stachenfeld, K. L., Botvinick, M. M. & Gershman, S. J. The hippocampus as a predictive map. *Nat. Neurosci.* **20**, 1643–1653 (2017).
29. Sarel, A., Finkelstein, A., Las, L. & Ulanovsky, N. Vectorial representation of spatial goals in the hippocampus of bats. *Science* **355**, 176–180 (2017).
30. Mauritz, K. H. & Wise, S. P. Premotor cortex of the rhesus monkey: neuronal activity in anticipation of predictable environmental events. *Exp. Brain Res.* **61**, 229–244 (1986).
31. Theeuwes, J., Kramer, A. F. & Irwin, D. E. Attention on our mind: the role of spatial attention in visual working memory. *Acta Psychol. (Amst.)* **137**, 248–251 (2011).
32. Kriegeskorte, N. Pattern-information analysis: from stimulus decoding to computational-model testing. *Neuroimage* **56**, 411–421 (2011).
33. Muller, R. U. & Kubie, J. L. The effects of changes in the environment on the spatial firing of hippocampal complex-spike cells. *J. Neurosci.* **7**, 1951–1968 (1987).
34. Leutgeb, S. et al. Independent codes for spatial and episodic memory in hippocampal neuronal ensembles. *Science* **309**, 619–623 (2005).
35. Burke, S. N. et al. The influence of objects on place field expression and size in distal hippocampal ca1. *Hippocampus* **21**, 783–801 (2011).
36. Hollup, S., Molden, S., Donnett, J., Moser, M. & Moser, E. Accumulation of hippocampal place fields at the goal location in an annular watermaze task. *J. Neurosci.* **21**, 1635–1644 (2001).
37. Suzuki, W. A., Miller, E. K. & Desimone, R. Object and place memory in the macaque entorhinal cortex. *J. Neurophysiol.* **78**, 1062–1081 (1997).
38. Weible, A. P., Rowland, D. C., Pang, R. & Kentros, C. Neural correlates of novel object and novel location recognition behavior in the mouse anterior cingulate cortex. *J. Neurophysiol.* **102**, 2055–2068 (2009).
39. Jacobs, J. et al. Direct electrical stimulation of the human entorhinal region and hippocampus impairs memory. *Neuron* **92**, 1–8 (2016).
40. Goyal, A. et al. Electrical stimulation in hippocampus and entorhinal cortex impairs spatial and temporal memory. *J. Neurosci.* **38**, 3049–17 (2018).
41. Braak, H. & Braak, E. Neuropathological stageing of alzheimer-related changes. *Acta Neuropathol.* **82**, 239–259 (1991).
42. Gomez-Isla, T. et al. Profound loss of layer II entorhinal cortex neurons occurs in very mild Alzheimer's disease. *J. Neurosci.* **16**, 4491 (1996).
43. Jacobs, H. I. L. et al. Structural tract alterations predict downstream tau accumulation in amyloid-positive older individuals. *Nat. Neurosci.* **21**, 424–431 (2018).
44. Maass, A. et al. Entorhinal tau pathology, episodic memory decline, and neurodegeneration in aging. *J. Neurosci.* **38**, 530–543 (2018).
45. Fu, H. et al. Tau pathology induces excitatory neuron loss, grid cell dysfunction, and spatial memory deficits reminiscent of early Alzheimer's disease. *Neuron* **93**, 533–541.e5 (2017).
46. Doeller, C. F., Barry, C. & Burgess, N. Evidence for grid cells in a human memory network. *Nature* **463**, 657–661 (2010).
47. Maidenbaum, S., Miller, J., Stein, J. M. & Jacobs, J. Grid-like hexadirectional modulation of human entorhinal theta oscillations. *Proc. Natl Acad. Sci. USA* **115**, 10798–10803 (2018).
48. Boccara, C. N., Nardin, M., Stella, F., O'Neill, J. & Csicsvari, J. The entorhinal cognitive map is attracted to goals. *Science* **363**, 1443–1447 (2019).
49. Constantinescu, A. O., O'Reilly, J. X. & Behrens, T. E. J. Organizing conceptual knowledge in humans with a gridlike code. *Science* **352**, 1464–1468 (2016).
50. Aronov, D., Nevers, R. & Tank, D. W. Mapping of a non-spatial dimension by the hippocampal–entorhinal circuit. *Nature* **543**, 719 (2017).

Methods

Task. Nineteen patients with drug-resistant epilepsy performed 31 sessions of a spatial memory task at their bedside with a laptop computer and handheld controller. This study was approved by the Institutional Review Boards of Columbia University, Columbia University Medical Center (New York, NY), Emory University (Atlanta, GA), University of Texas Southwestern (Dallas, TX), and Thomas Jefferson University (Philadelphia, PA). All participants provided written consent agreeing to participation in this experiment. In this virtual reality (VR) memory task, participants were moved from the beginning to the end of a linear track in each trial. The track was 68 VR-units long, which corresponds to approximately 231 meters when converted using the height of the virtual avatar relative to the environment and track length. The ground was textured to mimic asphalt and the track was surrounded by stone walls (Fig. 1a). In each trial participants were placed at the beginning of the track and shown text cues instructing them to press a button on the game controller when they reached the location of a specified object (instruction period). Immediately after receiving this cue, participants pressed a button on a game controller to move to the hold period, in which they were held stationary at the entrance to the track for 4 s. Next, the movement period began automatically, in which participants were moved forwards along the track. Participants were moved passively for 56 of 64 trials, and in the other, randomly selected, trials controlled movements with a handheld controller (Supplementary Fig. 1a). Individual trials consisted of either encoding or retrieval trials (see Fig. 1a). The first two times that participants encountered a particular object were encoding trials, in which the object was visible during movement so that participants could learn its location. In subsequent retrieval trials, the object was invisible and participants were instructed to recall its location by pressing the controller button when they believed they were at the correct location. To measure task performance, we computed the distance error for each trial, defined as the distance between the participant response location and the actual location of the object. Participants encoded and retrieved a total of four unique object–location associations (16 trials of each) over the course of a session, with each object located at a different randomly selected location (Fig. 1b). The temporal order and spatial order of objects were randomly associated, such that each object would be randomly be assigned to locations 1–4 independent of the temporal order of that object (that is, the first object in the session could be presented in the fourth location).

In addition to pressing a button to indicate their memory of the object location, participants were told to press a button as they entered the stopping zone at the end of the track, which is visually delineated by a red floor coloring at the end of the track. Pressing the button in this region ended the movement period, and participants were then shown a fixation cross for 5 s (fixation period).

Finally, during the feedback period at the end of each trial, participants received points corresponding to how close to the correct location they pressed the button during movement. Only one object was ever present on the track at any given time. The task was split into two blocks so that participants would only be cued to retrieve from either the first or second object in the first block versus the third or fourth object for the second block. After learning the location of an object during the encoding trials, participants were cued with that object for at least two consecutive trials before potentially being cued with the other object for that block (see Supplementary Fig. 1a).

A distinctive feature of our task was that, during movement periods, participants were moved passively while their speed was automatically changed in a seemingly random fashion. These uncontrolled speed changes encouraged participants to attend continuously to their current VR location because they could not accurately predict future positions by integrating their past velocity. Within each third of the track, participants were moved at a constant speed, which was randomly chosen from the range of 2–12 VR-units s^{-1}. The areas in which speed changes occurred are indicated in the schematic shown in Fig. 1b. When speed changes occurred, acceleration took place gradually over the course of 1 s to avoid a jarring transition.

Data recording. The participants in our study were epilepsy patients who had Behnke–Fried microelectrodes (Ad-Tech Medical) surgically implanted in the course of clinical seizure mapping[51] at four hospital sites: Emory University Hospital, University of Texas Southwestern Medical Center, Thomas Jefferson University Hospital, and Columbia University Medical Center. Microwire implantation and data acquisition largely followed previously reported procedures[13] and were approved by an institutional review board at all participating institutions, and informed consent was obtained from all participants. The depth electrodes featured 9 platinum–iridium microwires (40 µm) extending from the electrode tip and were implanted in target regions selected for clinical purposes. We recorded microwire data at 30 kHz using either the Cheetah (Neuralynx) or NeuroPort (Blackrock Microsystems) recording systems. Data collection and analysis were not performed blind to the conditions of the experiments. We used Combinato[52] for spike detection and sorting. We excluded neurons that had a mean firing rate of less than 0.2 Hz or more than 15 Hz (potential interneurons). Manual sorting identified single- versus multi-unit activity versus noise on the basis of previously determined criteria[53,54].

Microelectrode bundle localization followed a similar process to that described previously[39,55]. We determined the anatomic location of each implanted microwire electrode bundle using a combination of pre-implantation MRI and post-implantation computed tomography (CT) scans (Supplementary Fig. 2). First, we performed automated whole brain and MTL anatomic segmentation on T1-weighted (whole brain coverage, 3D acquisition, 1 mm isotropic resolution) and T2-weighted (temporal lobe coverage, coronal turbo spin echo acquisition, $0.4 \times 0.4 \times 2$ mm resolution) MRI[56,57].

A post-implantation CT scan was then co-registered to the MRI scans and a neuroradiologist identified the positions of electrode contacts and microwire bundles based on the source images and processed data[58]. Further detail regarding imaging parameters can be found in the Nature Research Reporting Summary.

Statistical analysis. No statistical methods were used to predetermine sample sizes, but our sample sizes are similar to those reported in previous publications[13,59]. For all omnibus testing (ANOVA) described in this study, we used a non-parametric permutation method to generate a large number of permutations in which observations are permuted within each block. This enabled us to determine critical statistics and P values (permutation adjusted) against empirically derived null distributions. False discovery rate (FDR) adjustment was used to correct for multiple comparisons where appropriate. Firing rate was z-scored within each session, omitting manual movement trials. Because overall z-scored firing rates may be subject to bias from stimulus-induced increases in firing rate, we computed the z-score after removing the spatial bin with the highest firing rate in each trial or spatial bins with $z > 3.29$ (exceeding the 99.9th percentile of the normal distribution).

Identifying place cells and memory-trace cells. To examine how neuronal activity varied with location in the virtual environment, we binned the virtual track into 40 bins, referred to as VR-bins (equivalent to 1.7 VR-units), enabling the measurement of neuronal firing rates in this binned space. For each cell, we counted the spikes in each spatial bin and divided this quantity by the time spent in that bin to yield a firing rate estimate. We smoothed this firing rate estimate on a single-trial level using a Gaussian kernel with a width of 8 VR-bins (± 4 VR-bins). We excluded the bins in which participants spent less than 100 ms over the course of the entire task. This excluded several bins in the stopping zone, because the movement period ended as soon as participants pressed the button in the stopping zone. We did not analyze data from the manual movement trials for this study.

We used a two-way repeated-measure ANOVA to examine the effects of participant location (1–40 VR-bins), object retrieval cue (1, 2, 3, 4), and their interaction, on the binned firing rate of each cell. After using ANOVA to screen cell responses, we defined individual spatial firing fields as contiguous bins in which firing rate exceeded a baseline threshold[21,36,60,61]. We determined this baseline threshold independently for each cell, using non-parametric permutation testing to build empirical estimates of the threshold by circularly shifting the firing rate estimates 500 times, re-binning the firing rate, and selecting the 95th percentile of the permuted distribution of firing rates.

We defined place cells as those cells that showed a significant main effect of location on firing rate via the ANOVA, and that also had a spatial firing field (place field) greater than 5% the size of the track. Additionally, we performed an ANCOVA to confirm the main effect of position in the ANOVA, with position serving as a main factor and speed and time as covariates[24]. This analysis used a 3 s window surrounding the response, as anticipatory motor responses occur within 1 s of a movement[30]. We only considered a neuron to be a place cell if its firing was significantly modulated by participant location even after factoring time and speed in as covariates in the ANCOVA. Additionally, six cells showed a main effect of object cue on firing rate. These cells were excluded from analyses. We defined memory-trace cells as those cells with a firing rate that showed an interaction between participant location and object cue in the ANOVA and that showed a significant spatial firing field (trace field) for at least one cue. A trace field for a particular object cue was considered unique if the peak location, in which firing rate was maximal, did not overlap with that of any other trace field for that cell.

Because all subsequent analyses relied on our characterization of place and memory-trace cells, we conducted a range of control analyses to ensure that the proportions of cells categorized as such was robust to: dependence between task sessions for individual patients, recordings from seizure-onset zones, changes in bin-size for spatial firing-rate estimates, and the statistical assumptions of our omnibus testing. These analyses and their results are summarized in Supplementary Table 2.

Correlation between encoding and retrieval firing rates. We computed the correlation between the spatial firing patterns of each memory-trace cell between retrieval and encoding trials to establish whether memory-trace cells fire in the same locations during these phases at different firing rates ('congruent') or whether they exhibited completely different firing patterns during these two phases ('incongruent'). Specifically, we limited this analysis to the blocks of trials in which the participant viewed a cue for which a memory-trace cell had a trace field, as these cells had trace fields for 1–4 of the cues. We assessed significance using a permutation procedure, comparing the actual correlation coefficient to the coefficient computed by applying the same procedure to randomly shuffled firing rate vectors. We then tested the significance of the proportion of cue conditions

showing congruent spatial firing between encoding and retrieval trace fields against the proportion showing incongruent spatial firing.

Assay of attention during encoding trials. We examined the effect of attention[62] on memory-trace cell activity. To assay attention, we relied on the fact that the object is visible during the encoding trials of the task. This visibility ensured that the performance of participants in these trials would depend primarily on how closely the participant was attending to their location in space. We therefore used the distance error of participants in encoding trials as a proxy measure for attention level. This assay allowed examination of the putative effect of attention on neural activity independently of memory retrieval. We therefore split encoding trials into low- and high-attention groups, based on whether the distance error between the button press and the visible object was greater or less than 1.5 VR-bins, respectively (determined via mean split). We performed a two-way ANOVA assessing how memory-trace cell activity during encoding was modulated by attention level in that trial (low or high) as well as the location of the trace field relative to the response.

Task period firing rate comparison. To compare the magnitude of pre- versus post-response firing rate changes to firing rates during different task periods, we computed the response period firing rate by normalizing the activity in the 10 VR-bins preceding the response by the 10 VR-bins following the response. This also helped to ensure that correlations computed between task periods and the response period (see Fig. 6) were not confounded by trial-wide increases in baseline firing rate. We used robust linear regression to examine the correlation between hold and response period activity (Fig. 6b,c). This approach minimizes the effect of outliers using iteratively re-weighted least squares with a bisquare weighting function[63].

To further verify that some other aspect of our chosen response period was not leading to artifactual correlation, we computed the correlation between the hold period firing rate and a matched control period. The control period was computed identically to the response period, but we used the regions of the track that did not overlap with the response period. In this way, the control period was of equal length to the response period, and the neural activity during this control period did not overlap with the neural activity during the response period to control for the effect of the response on firing rate.

Cross-decoding analysis. We used a multivariate cross-decoding framework to test whether memory-trace cell activity reflected information about each object–location memory across different retrieval contexts. A schematic for this framework is shown in Supplementary Fig. 13. To assess cross-decoding performance, we pooled the memory-trace cells recorded across all patients and sessions and constructed two pseudopopulations: entorhinal cortex memory-trace cells and non-entorhinal memory-trace cells. Pseudopopulation decoding has been used to describe the common neural dynamics of functionally similar subsets of cells without the inherent noise correlations shared by neurons recorded in the same session[59]. For each decoder, we used a k-nearest neighbors algorithm using a one-versus-all paradigm for multi-class decoding of the remembered item from the recorded neuronal activity. Firing rates were binned by task period and normalized. As detailed in the previous section, we computed the response period firing rate by normalizing the activity in the 10 VR-bins preceding the response by the 10 VR-bins following the response for each trial (Supplementary Fig. 13). We computed the response period firing rate for each trial, regardless of response accuracy. We also used a similar method to compute a matched control period, which was based on the 20 VR-bins that were not used to compute the response period activity.

For cross-decoding, each separate decoder was trained to predict the currently cued object–location memory from the normalized firing rates of the population of memory-trace cells for each of the task periods.

Each model was then tested on activity from a different period. In addition to our cross-decoding framework, we trained and tested decoders on the activity of the same period—these decoders were trained using leave-one-out cross-validation to assess performance (Supplementary Fig. 13). We assessed significant decoding accuracy using a binomial test. Chance-level decoding accuracy was 25%, as verified by shuffling all labels and reassessing the decoding performance across the 1,000 random permutations.

Reporting Summary. Further information on research design is available in the Nature Research Reporting Summary linked to this article.

Data availability

The data that support the findings of this study are available on reasonable request from the corresponding author. The data are not publicly available because they could compromise research participant privacy and consent.

Code availability

Task was coded using the publicly available programming library PandaEPL[64]. Analysis was performed in Matlab and spike sorting in Python using the publicly available software package Combinato[52]. Analysis code is available on reasonable request from the corresponding author.

References

51. Fried, I. et al. Cerebral microdialysis combined with single-neuron and electroencephalographic recording in neurosurgical patients. *J. Neurosurg.* **91**, 697–705 (1999).
52. Niediek, J., Boström, J., Elger, C. E. & Mormann, F. Reliable analysis of single-unit recordings from the human brain under noisy conditions: tracking neurons over hours. *PLoS One* **11**, e0166598 (2016).
53. Hill, D., Mehta, S. & Kleinfeld, D. Quality metrics to accompany spike sorting of extracellular signals. *J. Neurosci.* **31**, 8699–8705 (2011).
54. Valdez, A. B., Hickman, E. N., Treiman, D. M., Smith, K. A. & Steinmetz, P. N. A statistical method for predicting seizure onset zones from human single-neuron recordings. *J. Neural Eng.* **10**, 016001 (2013).
55. Lee, S. A. et al. Electrophysiological signatures of spatial boundaries in the human subiculum. *J. Neurosci.* **38**, 3265–3272 (2018).
56. Wang, H. et al. Multi-atlas segmentation with joint label fusion. *IEEE Trans. Pattern Anal. Mach. Intell.* **35**, 611–623 (2013).
57. Yushkevich, P. A. et al. Automated volumetry and regional thickness analysis of hippocampal subfields and medial temporal cortical structures in mild cognitive impairment. *Hum. Brain Mapp.* **36**, 258–287 (2015).
58. Avants, B. B., Epstein, C. L., Grossman, M. & Gee, J. C. Symmetric diffeomorphic image registration with cross-correlation: evaluating automated labeling of elderly and neurodegenerative brain. *Med. Image Anal.* **12**, 26–41 (2008).
59. Kamin´ski, J. et al. Persistently active neurons in human medial frontal and medial temporal lobe support working memory. *Nat. Neurosci.* **20**, 590–601 (2017).
60. Fyhn, M., Molden, S., Witter, M., Moser, E. & Moser, M. Spatial representation in the entorhinal cortex. *Science* **305**, 1258–1264 (2004).
61. Alme, C. B. et al. Place cells in the hippocampus: eleven maps for eleven rooms. *Proc. Natl Acad. Sci. USA* **111**, 18428–18435 (2014).
62. Wilming, N., König, P., König, S. & Buffalo, E. A. Entorhinal cortex receptive fields are modulated by spatial attention, even without movement. *Elife* **7**, e31745 (2018).
63. Holland, P. W. & Welsch, R. E. Robust regression using iteratively reweighted least-squares. *Commun. Stat. Theory Methods* **A6**, 813–827 (1977).
64. Solway, A., Miller, J. F. & Kahana, M. J. PandaEPL: a library for programming spatial navigation experiments. *Behav. Res. Methods* **45**, 1293–1312 (2013).

Acknowledgements

We are grateful to the patients for participating in our study. This work was supported by NIH grants R01-MH104606 (to J.J.) and S10-OD018211 (to C.S.), NSF grants BCS-1724243 and BCS-1848465 (to J.J.), and NSF Graduate Research Fellowship DGE 16-44869 (to S.E.Q.). We thank Andrew Watrous (University of Texas, Austin), Melina Tsitsiklis (Columbia University), Ida Momennejad (Columbia University), Mariam Aly (Columbia University), Nicole Long (University of Virginia), and Niko Kriegeskorte (Columbia University) for helpful comments and suggestions.

Author contributions

J.J. conceived the experiment; R.E.G., J.T.W., B.L., A.S., C.W., S.A.S., and G.M.M. performed surgical procedures; S.E.Q., J.M., M.R.S., C.S., E.H.S., J.-J.L., and C.S.I. performed data collection and recording; J.M.S. processed neuroimaging data; S.E.Q. analyzed the data; and S.E.Q. and J.J. wrote the manuscript.

Competing interests

The authors declare no competing interests.

Additional information

Supplementary information is available for this paper at https://doi.org/10.1038/s41593-019-0523-z.

Correspondence and requests for materials should be addressed to J.J.

Peer review information *Nature Neuroscience* thanks Stefan Leutgeb and other, anonymous, reviewer(s) for their contribution to the peer review of this work.

Reprints and permissions information is available at www.nature.com/reprints.

nature research

Corresponding author(s): Salman Qasim
Joshua Jacobs

Last updated by author(s): Sep 10, 2019

Reporting Summary

Nature Research wishes to improve the reproducibility of the work that we publish. This form provides structure for consistency and transparency in reporting. For further information on Nature Research policies, see Authors & Referees and the Editorial Policy Checklist.

Statistics

For all statistical analyses, confirm that the following items are present in the figure legend, table legend, main text, or Methods section.

n/a	Confirmed	
☐	☒	The exact sample size (*n*) for each experimental group/condition, given as a discrete number and unit of measurement
☐	☒	A statement on whether measurements were taken from distinct samples or whether the same sample was measured repeatedly
☐	☒	The statistical test(s) used AND whether they are one- or two-sided *Only common tests should be described solely by name; describe more complex techniques in the Methods section.*
☐	☒	A description of all covariates tested
☐	☒	A description of any assumptions or corrections, such as tests of normality and adjustment for multiple comparisons
☐	☒	A full description of the statistical parameters including central tendency (e.g. means) or other basic estimates (e.g. regression coefficient) AND variation (e.g. standard deviation) or associated estimates of uncertainty (e.g. confidence intervals)
☐	☒	For null hypothesis testing, the test statistic (e.g. *F*, *t*, *r*) with confidence intervals, effect sizes, degrees of freedom and *P* value noted *Give P values as exact values whenever suitable.*
☒	☐	For Bayesian analysis, information on the choice of priors and Markov chain Monte Carlo settings
☒	☐	For hierarchical and complex designs, identification of the appropriate level for tests and full reporting of outcomes
☐	☒	Estimates of effect sizes (e.g. Cohen's *d*, Pearson's *r*), indicating how they were calculated

Our web collection on statistics for biologists contains articles on many of the points above.

Software and code

Policy information about availability of computer code

Data collection	Task was coded using the publicly available programming library PandaEPL. Data was recorded using commercial software from BlackRock Microsystems (v 7.0.5.0) and Neuralynx (v 5.6.0).
Data analysis	Analysis was performed in Matlab (v 2015b) and spike sorting in Python using the publicly available code Combinato (no version #).

For manuscripts utilizing custom algorithms or software that are central to the research but not yet described in published literature, software must be made available to editors/reviewers. We strongly encourage code deposition in a community repository (e.g. GitHub). See the Nature Research guidelines for submitting code & software for further information.

Data

Policy information about availability of data

All manuscripts must include a data availability statement. This statement should provide the following information, where applicable:

- Accession codes, unique identifiers, or web links for publicly available datasets
- A list of figures that have associated raw data
- A description of any restrictions on data availability

The data that support the findings of this study are available on reasonable request from the corresponding author. The data are not publicly available because they could compromise research participant privacy/consent.

Field-specific reporting

Please select the one below that is the best fit for your research. If you are not sure, read the appropriate sections before making your selection.

☒ Life sciences ☐ Behavioural & social sciences ☐ Ecological, evolutionary & environmental sciences

For a reference copy of the document with all sections, see nature.com/documents/nr-reporting-summary-flat.pdf

Life sciences study design

All studies must disclose on these points even when the disclosure is negative.

Sample size	No statistical methods were used to pre-determine sample sizes but our sample sizes are similar to those reported in previous publications.
Data exclusions	Individual cells were excluded based on standard criteria for recording quality, described in the Methods. Spike sorting was done using Combinato, which uses a technique called super-paramagnetic clustering to identify potential waveform clusters based on recorded threshold-crossings. Then, the algorithm over-clusters and performs iterative template-matching to yield putative single-units. After identifying putative single-unit activity, we excluded neurons that had a mean firing rate below 0.2 Hz or above 15 Hz (potential interneurons).
Replication	Findings replicated across multiple subjects, and findings also replicated from multiple sessions within some subjects.
Randomization	Subjects were all allocated into one group for analysis.
Blinding	Data collection and analysis were not performed blind to the conditions of the experiments. Blinding was not relevant to our study. The data collected requires many processing steps to become interpretable, so there is no way for the experimenter to be biased during data collection by results coming in.

Reporting for specific materials, systems and methods

We require information from authors about some types of materials, experimental systems and methods used in many studies. Here, indicate whether each material, system or method listed is relevant to your study. If you are not sure if a list item applies to your research, read the appropriate section before selecting a response.

Materials & experimental systems

n/a	Involved in the study
☒	☐ Antibodies
☒	☐ Eukaryotic cell lines
☒	☐ Palaeontology
☒	☐ Animals and other organisms
☐	☒ Human research participants
☒	☐ Clinical data

Methods

n/a	Involved in the study
☒	☐ ChIP-seq
☒	☐ Flow cytometry
☐	☒ MRI-based neuroimaging

Human research participants

Policy information about studies involving human research participants

Population characteristics	All subject demographic information is in Supplementary Table 1 of the manuscript. Briefly, all subjects were patients undergoing surgical treatment for epilepsy. We included data from 19 such patients (13 male, 6 female). Mean age was 34.1 years, with a standard deviation of 11.9 years.
Recruitment	Subjects were recruited from the pool of epilepsy patients between the ages of 18 and 65 years, with close to normal neuropsych evaluation, who were undergoing chronic implantation of subdural and/or intracortical electrodes with long term EEG recording for clinical purposes. It is possible that self-selection bias may be present, i.e. patients with depression or low-motivation levels may have opted out of research, but we do not believe this affected our electrophysiological findings.
Ethics oversight	Study protocol was approved by IRB at Emory University Hospital (Atlanta, GA), UT Southwestern Medical Center (Dallas, TX), Thomas Jefferson University Hospital (Philadelphia, PA), and Columbia University Medical Center (New York, NY).

Note that full information on the approval of the study protocol must also be provided in the manuscript.

Magnetic resonance imaging

Experimental design

Design type	MRI were acquired purely for clinical purposes to indicate electrode placement, and were not a part of the experiment.
Design specifications	MRI were acquired purely for clinical purposes to indicate electrode placement, and were not a part of the experiment.
Behavioral performance measures	MRI were acquired purely for clinical purposes to indicate electrode placement, and were not a part of the experiment.

Acquisition

Imaging type(s)	Structural MRI and CT
Field strength	3T MRI - before electrode implantation, 1.5 T MRI - after implantation
Sequence & imaging parameters	Sequence & imaging parameters: Imaging parameters varied somewhat among institutions in this multisite study. In general, sequences required for macroelectrode and microwire localization included 3D T1-weighted with 1 mm or less isotropic resolution, coronal fast spin echo T2-weighted with 0.4 x 0.4 mm in-plane resolution and 2 mm slice thickness, and CT with less than 1 mm slice thickness. Representative examples are as follows: Pre-implant 3D T1-weighted MPRAGE (TR 1900 ms, TE 2.52 ms, flip angle 9, 1 mm isotropic resolution, 216 x 256 x 174 matrix), pre-implant coronal FSE T2-weighted (TR 7200 ms, 76 ms, ETL 15, flip angle 139, 0.4 x 0.4 x 2 mm, 448 x 448 x 30), post-implant CT (0.5 x 0.5 x 0.625 mm, 512 x 512 x 384).
Area of acquisition	T1 - whole brain, T2 - temporal lobes spanning and oriented perpendicular to the hippocampal long axis

Diffusion MRI ☐ Used ☒ Not used

Preprocessing

Preprocessing software	Segmentations of hippocampal subfields and parahippocampal cortical regions including the entorhinal cortex were generated from 3D T1-weighted and coronal T2-weighted images using Automatic Segmentation of Hippocampal Subfields (ASHS) software.
Normalization	Pre-implant MRI, post-implant CT, and when available post-implant MRI scans were all aligned to each other using rigid registration based on mutual information with Advanced Normalization Tools (ANTS) softwar
Normalization template	No normalization template was used.
Noise and artifact removal	No noise or artifact removal was used.
Volume censoring	No volume censoring was used.

Statistical modeling & inference

Model type and settings	No statistical modeling was used as MRI were acquired for clinical purposes to indicate electrode placement.
Effect(s) tested	No effects tested as MRI were acquired for clinical purposes to indicate electrode placement.

Specify type of analysis: ☐ Whole brain ☒ ROI-based ☐ Both

Anatomical location(s)	Pre and post-implant MRI and post-implant CT scans were co-registered based on maximal mutual information using ANTS software. Segmentations of hippocampal subfields and parahippocampal cortical regions including the entorhinal cortex were generated from 3D T1-weighted and coronal T2-weighted images using Automatic Segmentation of Hippocampal Subfields (ASHS) software.
Statistic type for inference (See Eklund et al. 2016)	No inference was done as MRI were acquired for clinical purposes to indicate electrode placement.
Correction	No correction was used as MRI were acquired for clinical purposes to indicate electrode placement.

Models & analysis

n/a	Involved in the study
☒	☐ Functional and/or effective connectivity
☒	☐ Graph analysis
☒	☐ Multivariate modeling or predictive analysis